Submitted for the Proceedings of ESA Living Planet Symposium, Prague, 9-13 May 2016, ESA-SP 740

PARTICULATE BACKSCATTERING AND SUSPENDED MATTER CONCENTRATION RETRIEVAL FROM REMOTE-SENSED TURBIDITY IN VARIOUS COASTAL AND RIVERINE TURBID WATERS

Bouchra Nechad [(1)], Ana Dogliotti [(2)], Kevin Ruddick[(1)], David Doxaran [(3)]

[(1)]Royal Belgian Institute of Natural Sciences, Operational Directorate Natural Environment, Belgium. Email: bnechad@naturalsciences.be
[(2)]Instituto de Astronomía y Física del Espacio (IAFE), CONICET/UBA, Argentina. Email: adogliotti@iafe.uba.ar
[(3)]Laboratoire d'Océanographie de Villefranche (LOV), UMR7093, CNRS/UPMC, France. Email: doxaran@obs-vlfr.fr

ABSTRACT

The semi-empirical algorithm of [1] for the estimation of turbidity (*T*) from marine reflectance (*Rrs*) is calibrated and validated using a large dataset of *in situ* measurements collected in various waters, for use with any ocean colour hyperspectral sensor, and with Sentinel-2, Landsat 8 and Pléiades spectral bands. The relationship between particulate backscattering coefficient (b_{bp}) and side-scattering (*T*) is investigated through simulation of Fournier-Forand phase functions, assuming variable particles size and composition. Two algorithms for the estimation of b_{bp} at 850nm and suspended particulate matter (*SPM*) from turbidity are proposed, and calibrated and validated using *T*, b_{bp} and *SPM* in situ measurements in clear to extremely turbid waters.

1. INTRODUCTION

In-water suspended particulate matter concentrations (SPM) is of interest in various oceanographic research fields (e.g. underwater light attenuation and visibility, sediment transport modelling) and can be mapped from satellites.

Since several decades, remote sensing algorithms have been developed to retrieve SPM from marine reflectance (ρ_w) in open ocean case 1 waters, and later in coastal waters with complex optics. However, these algorithms show large uncertainties when applied to waters with specific inherent optical properties (SIOPs) different from those assumed in the algorithms.

Water turbidity, T, a measurement of particles side-scattering, has been demonstrated to be not only a good proxy to SPM [2], but also to be highly correlated to marine reflectance in the red and near infrared spectral ranges, e.g. [1]. Moreover, Dogliotti et al. (2015) [3] found that the relationship between T and Rrs is only weakly sensitive to the natural variability of SIOPs and to the particulate scattering phase function.

2. DATA AND METHOD

Above water and in-water measurements have been carried out in various coastal waters around the world from 2007 to 2015 (Fig. 1): the southern North Sea (SNS) -including measurements in the Scheldt Estuary (SC est.) and in the Belgian port of Zeebrugge (ZB)-, the Mediterranean Sea (MS), the Scheldt River (SC), the Gironde (GR) and Río de la Plata (RP) estuaries and in the French Guiana coastal waters (FG). Supplementary in water measurements were performed in Belgium and France: in May 2015, at the Senne Canal (S1) and Senne River (S2) located in Machelen, north of Brussels, and at two pontoons along the Scheldt River denoted P1 (in Kallebeek), and P2 (in Antwerp), in July 2015 at MOW1 located in the southeast of the port of Zeebrugge, in the SNS; during February 2016, in the Rhône River plume (denoted RE), south of France (Fig. 1). A summary of measurements per site is given in Tab. 1.

2.1. Radiometric measurements

Radiometric measurements were performed simultaneously with water sampling and/or in water measurements in the southern North Sea using the above-water Trios (Rastede, Germany) Optical Systems (TRIOS), composed of three RAMSES hyper-spectral spectroradiometers, where simultaneous measurements of the above-water downwelling irradiance (*Ed*), the upwelling radiance (*Lsea*) and the sky radiance (*Lsky*) were acquired to estimate the water-leaving reflectance (ρ_w) as $\rho_{w=}$ *(Lsea- rf Lsky)/Ed=Lw/Ed*, where *rf* accounts for the fraction of refracted *Lsky* at air-sea interface (Fresnel reflectance), and is estimated from wind speed [4] in clear sky conditions, and set to 0.0265 in overcast conditions [5]. The sites FG, MS [6], SC, GR and RP [3], were also monitored using the same radiometric instruments, following the protocol of [5]. A set of 338 measurements were available after further quality-control of the data to insure low variability of sky conditions and of the water mass: the coefficient of variation, CV coefficients (defined as the ratio of the standard deviation by the average) of *Lsky/Ed*, *Lsky*, *Lw* and ρ_w over the 5 best scans selected at each station, are less than 25%.

2.2. In water measurements

Simultaneously with radiometric measurements, samples were collected for estimation of T and SPM at stations within the sites in Tab. 1.a. Turbidity and SPM measurements are further quality checked using the criteria 0.5 < SPM/T < 1.5 g m^{-3} FNU^{-1}. Turbidity measurements and in water continuous measurements of optical side- and back-scattering were performed at the sites listed in Tab. 1.b.

Turbidity was obtained using the portable HACH 2100P/Q ISO7027 (1999) turbidimeters which measure the ratio of light emitted at 860nm and scattered at 90° to the transmitted light, this turbidity is given in Formazin Nephelometric units (FNU).

In water continuous measurements were carried out using the following optical instruments:
- Hydroscat-4 (HOBI Labs), denoted by HS4, measures the spectral backscattering coefficients b_b (m^{-1}) over scattering angles [100°-160°] centered around 140°, and at four wavelengths. In this paper, only b_{b850} (at 850nm) is used, for comparison with OBS b_{bB} measurements.
- The optical backscatter OBS500 (Campbellsci), referred to hereafter by OBS, measures the side-scattering (b_s, at 90°) and backscattering (b_{bB}, between 125° and 170°) in Formazin Backscatter Units (FBU), using a LED emitting light at 860nm.
- The Laser In Situ Scattering and Transmissometry, LISST-100X type C (Sequoia Scientific), is used for the estimation of particles size distribution (PSD). Note that the LISST was deployed only at the Rhône River plume site.

The OBS provides average values and standard deviations, minima and maxima for b_s and b_{bB} over 1 min. The HS4 was set to measure b_b at a rate of 2 scans per second. These data were further quality controlled and processed to a) reject the first and last scans at each station and measurements taken at less than 10 cm depth (remove bubbles affect), b) correct HS4 for particles absorption along photon pathlength, using the improved sigma-correction method for turbid waters [7], c) reject negative or unrealistic data, and average HS4 data over 1 min windows, d) remove OBS and HS4 data with high coefficient of variation, CV, exceeding 25% over 1 min window, where CV is defined as the ratio of the standard deviation by the average value. The last mentioned quality control mainly removes air bubbles effects due to emerging or moving the sensor out of the water.

The random shape inversion matrix was used to estimate the volume concentration ([VC_i] in µl/l) from LISST measurements, in each size class *i*. The Junge parameter, γ, was computed following [6], with the number of particles, N(D_i) in a given size class *i* estimated from [VC_i], the particles diameter (D_i) and size classes $\Delta D_i = D_i - D_{i-1}$ ($2 \le i \le 31$) as follows [8]:

$$N(D_i) = \frac{[VC_i]}{\frac{3}{4}\pi D_i^{\,3}\Delta D_i} \times 10^{24} \qquad (1)$$

Table 1: a) Stations above- and in-water measurements sites, years, parameters, their $Median_{min}^{max}$ *values, and number of stations (N); b) Continuous in-water monitoring sites, years, parameters, their* $Median_{min}^{max}$ *values, and number of days of measurement (D).*

Site	Year(s)	$\rho_w 10^{-3}$ 780nm	SPM (g m^{-3})	T (FNU)	N
FG	2009	$8.0^{64.5}_{3.1}$	$14.1^{144.7}_{4.2}$	$13.9^{171.8}_{4.9}$	26
GR	2012, 2013	$118.2^{165.4}_{25.9}$	$455.7^{1525.0}_{68.0}$	$551.9^{1484.7}_{57.9}$	44
MS	2009	$0.7^{2.7}_{0.3}$	$0.6^{1.7}_{0.4}$	$0.7^{2.0}_{0.4}$	11
SC	2007-2015	$49.5^{76.5}_{20.7}$	$167.8^{347.0}_{49.6}$	$161.3^{365.0}_{48.1}$	23
SCest	2007-2015	$11.7^{14.7}_{8.1}$	$11.6^{26.13}_{7.6}$	$12.4^{25.3}_{8.2}$	5
SNS	2007-2015	$11.1^{71.0}_{0.6}$	$15.5^{151.3}_{0.6}$	$18.3^{180.0}_{0.7}$	168
ZB	2007-2015	$17.8^{32.7}_{6.4}$	$12.7^{26.7}_{7.1}$	$14.1^{28.3}_{7.4}$	9
RP	2012, 2015	$42.6^{64.3}_{27.4}$	$71.5^{159.2}_{41.7}$	$87.6^{185.8}_{62.1}$	52

Site	Year, D	b_s (FBU)	b_{bB} (FBU)	b_{b850} (%) (m^{-1})	T (FNU)	γ
RP	2015, 5	$59.0^{123.2}_{33.1}$	$40.4^{78.8}_{25.5}$	$51.0^{98.6}_{33.0}$	$57.9^{110.3}_{38.9}$	-
RE	2016, 2	$17.3^{53.0}_{1.6}$	$9.3^{30.1}_{0.2}$	$9.3^{37.5}_{0.6}$	$25.9^{64.7}_{1.5}$	$3.08^{3.56}_{2.63}$
SR1	2015, 1	$1.7^{3.5}_{0.8}$	$0.8^{1.3}_{0.4}$	$2.3^{2.9}_{1.9}$	$3.6^{3.8}_{2.7}$	-
SR2	2015, 1	$34.9^{50.8}_{12.0}$	$23.0^{36.8}_{8.5}$	$30.5^{42.7}_{12.7}$	$29.8^{51.0}_{15.6}$	-
P1	2015, 1	$135.4^{164.9}_{71.5}$	$80.5^{95.6}_{44.0}$	$107.3^{127.3}_{57.2}$	$149.0^{179.5}_{84.1}$	-
P2	2015, 1	$148.7^{269.3}_{72.6}$	$85.6^{148.3}_{43.7}$	$107.2^{214.6}_{53.6}$	$174.0^{240.0}_{90.3}$	-
MOW1	2015, 1	$32.4^{114.5}_{7.4}$	$19.6^{66.4}_{4.0}$	$25.5^{89.2}_{6.8}$	$40.5^{74.3}_{11.8}$	-

2.3.Turbidity model calibration

Using the turbidity model [1], type II linear regression analysis are performed on a subset of 162 turbidity and TriOS hyperspectral $\rho_w(\lambda_i)$ measurements, for λ_i ranging from 550 to 885nm, with a step of 2.5nm, and on a similar subset where TriOS reflectance spectra were convoluted with Sentinel-2 MSI, Pléiades and Landsat8-OLI sensors spectral response functions. To apply linear regression analysis, the independent variable $\rho_w(\lambda)$ is transformed into $X(\lambda)$ as follows:

$$X(\lambda) = \frac{\rho_w(\lambda)}{1 - \rho_w(\lambda)/\mathrm{C}(\lambda)} \qquad (2)$$

with values of C(λ) set as tabulated in [1], and set equal to 1.20 times the maximum reflectance measured, if these latter exceed values in [1] (to avoid model reaching its asymptote). The model is re-written as:

$$T = A(\lambda)X(\lambda) + B(\lambda) \qquad (3)$$

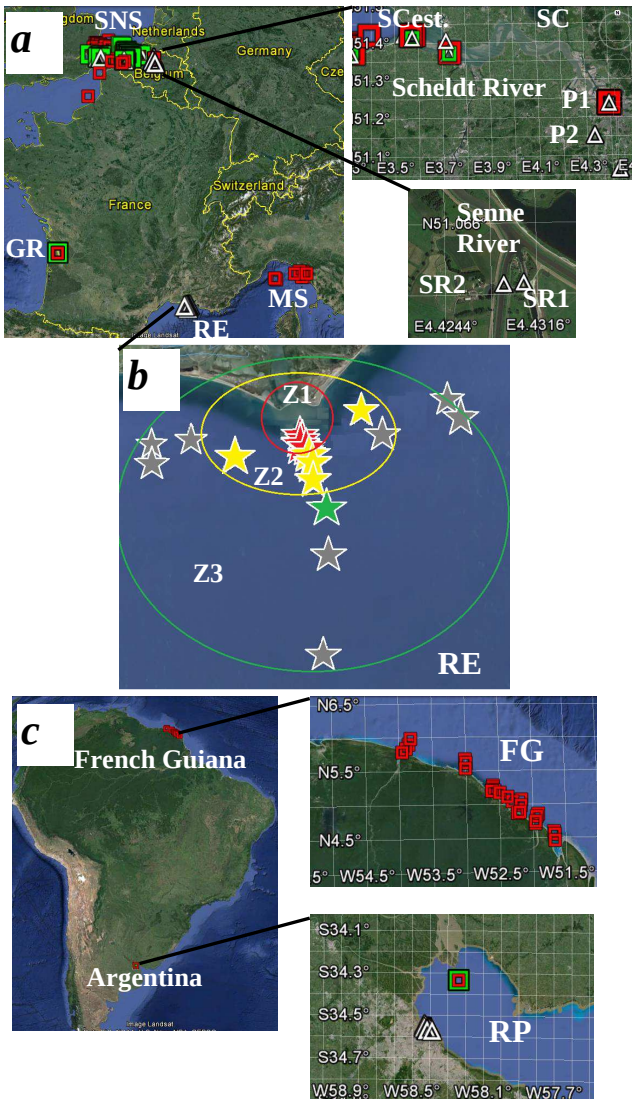

Figure 1. The locations of measurements within a) SNS, SC est., SC, GR, MS sites monitored from 2007 to 2015 (a, right), in the Senne and Scheldt Rivers on May 2015 (a, left), and of RE (Rhône River plume) on February 2016; b) RE site (zoomed): the red, yellow and green stars represent stations where simultaneous measurements of OBS and LISST are available (different colours used for different distances from the River mouth), the grey colour is where only LISST measurements are available. The ellipses delimit the three zones Z1, Z2 and Z3 (see text for details); and c) FG and RP sites, with the red (green) squares showing locations of reflectance and turbidity measurements used for calibration (validation) of turbidity algorithm, and the white triangles the locations of LISST, OBS and HS4 measurements.

To validate the calibrated model, the second subset of 176 measurements of T and $\rho_w(\lambda_i)$ is used, if which 87% (153 measurements) correspond to T>10 FNU.

2.4. Fournier-Forand simulations

Fournier-Forand simulations are performed to obtain volume scattering functions (VSF) for refractive indices, r_i, varying in 1.01 to 1.54 encompassing the ranges of inorganic and organic particles [9], and for Junge coefficients, γ, in [3.1-5.0], covering the ranges found in case1 and case2 waters [6]. From these simulations, assuming spherically shaped particles, the ratio b_s/b_b is obtained at each couple (r_i,γ). The aim is to examine the distribution of the modelled b_s/b_b versus (r_i,γ), to understand the distribution of the *in situ* b_s/b_{bB} versus the Junge parameter estimated from LISST measurements.

3. RESULTS AND DISCUSSION

The results of turbidity algorithm calibration and validation are presented (3.1), the relationships between the side- and back-scattering coefficients are addressed for the different field measurements (3.2), and the variation of the b_s/b_b ratio is investigated from *in situ* measurements and Fournier-Forand simulations (3.3).

3.1. Turbidity model results

Tab. 2 lists the calibration coefficients A and B, the coefficient C and the coefficient of determination of the goodness of fit of the regression curves, R^2, for the turbidity model (Eq. 2-3), for wavelengths ranging from 600 to 885nm. A similar table is provided for the bands of the three sensors Sentinel2-MSI, Pléiades and Landsat-8 OLI (Tab. 3).
The hyperspectral calibration gives the best fitting curves for T and associated ρ_w in the near infrared (NIR) spectral ranges 720-730nm and 790-820nm, with $R^2 \geq 93\%$.

The validation of the models using the full range of the validation subset yields mean absolute percentage errors (MAPE) higher than 45%, for all wavelengths, because of the larger scatter of data in the low turbidity range (due to higher reflectance measurements uncertainties in clearer waters). When the validation is performed using the reduced subset over T>10 FNU, MAPE decreases to 33-34% at 720-732.5 nm and to 32-34% to 777.5-825nm. An example of calibration curve and validation is shown in Fig. 2. At shorter wavelengths λ<690nm, the effects of absorption by algae particles on reflectance decrease the performance of the turbidity model that assumes low variability of particles backscattering to absorption ratio [3]. At longer wavelengths λ >830nm, the uncertainties of reflectance measurements likely due to Fresnel correction propagate to the turbidity model.

3.2. Side- and back-scattering measurements

The OBS side-scattering b_s and HACH turbidity (T) measurements are highly correlated, at all sites (not shown here).

Table 2: The calibration coefficient A and B, and R², and the adjusted C-coefficient. The standard deviation of A and B are reported between brackets.

λ (nm)	A	B	C	R²(%)
660	610.33 (40.32)	0 (0.51)	0.2418	81.7
662.5	602.06 (39.68)	0 (0.51)	0.2398	82.7
665	602.49 (39.46)	0 (0.64)	0.2385	83.2
667.5	602.04 (39.08)	0 (0.72)	0.2375	83.6
670	586.83 (37.81)	0 (0.67)	0.2365	84.1
672.5	580.84 (37.44)	0 (0.67)	0.2355	84.3
675	594.19 (38.73)	0 (0.58)	0.2343	84.0
677.5	623.20 (41.06)	0 (0.35)	0.2332	83.2
680	633.80 (43.97)	0 (0.44)	0.2317	83.0
682.5	627.41 (46.35)	0 (0.48)	0.2317	83.3
685	619.98 (47.10)	0 (0.47)	0.2321	83.7
687.5	612.80 (46.32)	0 (0.47)	0.2322	84.3
690	609.87 (43.04)	0 (0.42)	0.2320	85.0
692.5	615.55 (37.18)	0 (0.38)	0.2301	85.8
695	626.27 (33.67)	0 (0.48)	0.2282	86.6
697.5	639.49 (35.03)	0 (0.55)	0.2264	87.3
700	654.27 (38.30)	0 (0.49)	0.2247	88.1
702.5	528.56 (49.86)	0 (0.58)	0.1872	89.6
705	522.73 (52.37)	0 (0.62)	0.1879	91.6
707.5	521.87 (58.57)	0 (0.71)	0.1886	92.6
710	498.52 (11.85)	0 (0.72)	0.1892	93.1
712.5	547.59 (56.05)	0 (0.73)	0.1898	93.5
715	560.06 (49.43)	0 (0.73)	0.1904	93.6
717.5	665.37 (56.63)	0 (0.70)	0.1913	93.9
720	687.29 (55.65)	0 (0.75)	0.1922	94.0
722.5	753.22 (64.09)	0 (0.56)	0.1930	94.1
725	864.69 (55.79)	0 (0.56)	0.1937	94.1
727.5	959.93 (67.20)	0 (0.54)	0.1944	93.9
730	1033.99 (69.97)	0 (0.48)	0.1951	93.6
732.5	1191.61 (65.23)	0 (0.37)	0.1957	93.2
735	1317.80 (59.07)	0 (0.36)	0.1963	92.7
737.5	1403.26 (53.56)	0 (0.36)	0.1968	92.4
740	1466.93 (48.93)	0 (0.35)	0.1973	92.1
742.5	1494.51 (46.10)	0 (0.39)	0.1978	91.9
745	1526.93 (44.16)	0 (0.36)	0.1983	91.7
747.5	1522.65 (42.17)	0 (0.36)	0.1988	91.7
750	1515.23 (40.32)	0 (0.37)	0.1992	91.6
752.5	1513.64 (40.18)	0 (0.37)	0.1996	91.5
755	1523.37 (38.35)	0 (0.41)	0.2000	91.4
757.5	1529.78 (42.22)	0 (0.39)	0.2003	91.6
760	1447.67 (48.99)	0 (0.37)	0.2007	91.8
762.5	1449.74 (49.61)	0 (0.30)	0.2010	92.0
765	1468.30 (45.36)	0 (0.34)	0.2013	92.3
767.5	1592.44 (36.71)	0 (0.32)	0.2021	92.1
770	1590.14 (33.43)	0 (0.35)	0.2028	92.1
772.5	1562.97 (33.13)	0 (0.38)	0.2034	92.2
775	1546.31 (35.25)	0 (0.36)	0.2040	92.1
777.5	1519.32 (36.45)	0 (0.30)	0.2045	92.2
780	1504.84 (37.92)	0 (0.30)	0.2050	92.3
782.5	1484.38 (39.27)	0 (0.30)	0.2054	92.4
785	1489.98 (39.93)	0 (0.21)	0.2059	92.5
787.5	1456.32 (41.80)	0 (0.32)	0.2062	92.6
790	1419.75 (44.27)	0 (0.31)	0.2066	92.8
792.5	1401.95 (46.03)	0 (0.32)	0.2069	92.9
795	1371.08 (48.14)	0 (0.35)	0.2072	93.0
797.5	1369.85 (47.30)	0 (0.25)	0.2075	93.2
800	1346.02 (48.79)	0 (0.29)	0.2078	93.3
802.5	1319.45 (49.27)	0 (0.35)	0.2080	93.3
805	1328.95 (48.12)	0 (0.36)	0.2082	93.4
807.5	1317.21 (50.14)	0 (0.31)	0.2085	93.4
810	1312.75 (50.66)	0 (0.29)	0.2087	93.4
812.5	1306.83 (49.70)	0 (0.21)	0.2089	93.4
815	1325.71 (48.05)	0 (0.23)	0.2091	93.4
817.5	1340.79 (47.26)	0 (0.28)	0.2092	93.4
820	1423.76 (45.08)	0 (0.18)	0.2094	93.2
822.5	1491.32 (39.77)	0 (0.15)	0.2096	92.9
825	1594.83 (28.75)	0 (0.22)	0.2097	92.5
827.5	1704.18 (8.07)	0 (0.43)	0.2099	92.0
830	1823.92 (20.40)	0 (0.37)	0.2100	91.4
832.5	1996.58 (14.88)	0 (1.24)	0.2101	90.8
835	2241.38 (72.12)	0 (2.30)	0.2103	89.9
837.5	2691.00 (27.78)	0 (1.52)	0.2104	88.0
840	2482.85 (48.12)	0 (0.82)	0.2105	88.8
842.5	2383.49 (36.95)	0 (0.84)	0.2106	88.9
845	2726.11 (39.58)	0 (2.22)	0.2107	87.8
847.5	3024.10 (29.06)	0 (1.18)	0.2108	86.4
850	2926.22 (41.66)	0 (0.48)	0.2109	86.8
852.5	2823.00 (51.04)	0 (0.76)	0.2110	87.3
855	2813.13 (53.99)	0 (0.64)	0.2111	87.2
857.5	2782.81 (55.39)	0 (0.56)	0.2112	87.2
860	2763.85 (57.04)	0 (0.61)	0.2113	87.2
862.5	2648.53 (68.59)	0 (1.25)	0.2114	87.2
865	2654.07 (78.80)	0 (2.00)	0.2115	87.1
867.5	2698.39 (44.56)	0 (1.05)	0.2116	86.9
870	2756.48 (41.25)	0 (1.49)	0.2117	86.5
872.5	2778.25 (48.37)	0 (0.67)	0.2119	86.2
875	2722.49 (32.51)	0 (0.28)	0.2120	85.9
877.5	2786.85 (28.98)	0 (0.37)	0.2121	85.4
880	2841.44 (21.94)	0 (0.51)	0.2122	84.9
882.5	2893.28 (13.53)	0 (0.61)	0.2123	84.4
885	2898.37 (5.37)	0.10 (0.50)	0.2124	83.7

Table 3: The calibration coefficient A and B, and R², and the adjusted C-coefficient for Sentinel-2, Pléiades and Landsat8.

Satellite	Band	A	B	C	R²(%)
Sentinel-2	*560*	*228.72 (-33.38)*	*0 (-5.08)*	*0.2200*	*56.8*
	665	610.94 (-55.66)	0 (-0.89)	0.2324	82.0
	705	416.32 (-61.48)	0 (-0.60)	0.1875	91.8
	740	1547.25 (-50.27)	0 (-0.41)	0.1974	91.8
	782	1587.80 (-41.10)	0 (-0.34)	0.2053	92.3
	835	1858.22 (-17.55)	0 (-0.34)	0.1913	91.2
	865	3030.32 (-53.10)	0 (-0.51)	0.2115	86.5
Pléiades	*556*	*244.87 (-34.71)*	*0 (-5.07)*	*0.2148*	*57.0*
	645	575.27 (-51.99)	0 (-1.23)	0.2360	78.3
	828	1864.45 (-17.99)	0 (-0.34)	0.1932	91.2
	657	639.43 (-62.73)	0 (-2.04)	0.2034	68.3
Landsat8	*561*	*234.55 (-35.60)*	*0 (-4.72)*	*0.2217*	*57.8*
	591	*499.30 (-53.52)*	*0 (-2.78)*	*0.2256*	*59.6*
	654	526.82 (-37.10)	0 (-1.10)	0.2365	82.5
	864	3031.75 (-53.76)	0 (-0.50)	0.2114	86.5

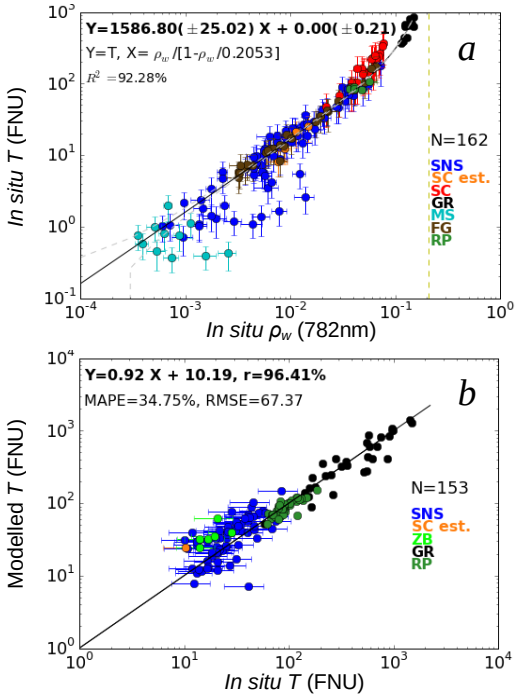

Figure 2. a) T model curve superimposed to in situ *turbidity versus* in situ *reflectance at Sentinel-2 MSI band 782nm; b) the modelled T versus* in situ *T, and associated regression line. The colours follow the colour of sites in the key.*

The backscatter coefficients b_{bB} and b_{b850} measured respectively by OBS and HS4 exhibit very good agreement during continuous measurements, at the Senne (SR1, SR2), Scheldt pontoon (P1, P2) and Río de la Plata River sites (Fig. 3).

The b_{bB} and b_b from all sites (Fig.4.a) have a strong correlation r=0.99. Except for measurements in the clearest waters (b_{bB}<2 FBU), the two backscattering coefficients are linearly related. The OBS b_{bB} measured

at 860nm, integrated over a range of scattering angles slightly different than the scattering angles of HS4, and calibrated in reference to Formazin, is convertible to the b_{b850} (in m^{-1}) through the relationship: b_{bB}=76.6 b_{b850}+0.06 (MAPE=6.4% for 0.2≤b_{bB}≤200 FBU), with MAPE dropping below 5% for b_{bB}≥10 FBU.

The ratio b_s/b_{bB} from continuous measurements varies significantly within each site, and between the sites: its median values range from 1.46 in Río de la Plata and the Senne River (SR2) to 2.15 in the Senne Canal, while very similar values (~1.70) are found in the SNS and the Scheldt River, and slightly higher value (1.90) at the Rhône River plume site. The average b_s/b_{bB} for all sites is 1.72.

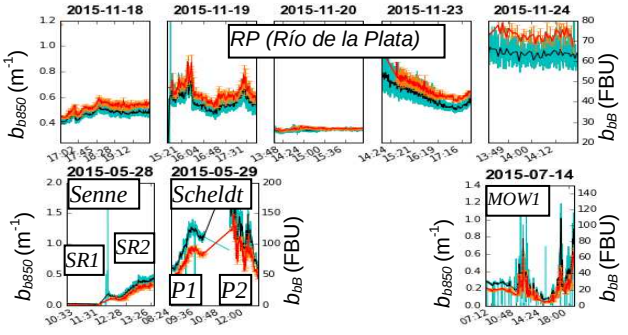

Figure 3. Continuous 1min-averaged measurements of b_{bB} and b_{b850}, respectively in red and black, and their standard deviations in orange and cyan, at Río de la Plata (top), the Senne (SR1, SR2) and Scheldt (P1, P2) locations (bottom left) and at MOW1 (bottom right).

Fig.4.b shows the variability of b_s/b_{bB} in terms of b_s. At high turbidity ranges (b_s>30 FBU) b_s/b_{bB} generally increases with increasing b_s. In clearer waters (b_s<2 FBU), the OBS backscattering coefficient approaches zero, yielding larger uncertainties in the estimated b_s/b_{bB}. In the medium turbidity range (2 to 30 FBU) the ratio spans 3 folds from 1.2 to 3.0, where higher ratio values are associated to lower turbidity.

In the following, the ratio b_s/b_{bB} at the Rhône River plume site is examined, as regards the spatial distribution (indicating particles type/composition) and particle size distribution.
The ratio b_s/b_{bB} is highly correlated with b_s, in the low range b_s <20 FBU (Fig.5.a), increasing from 1.36 to 2.43. For higher turbidity b_s ≥20 FBU, b_s/b_{bB} varies slightly around 1.8.

The general distribution of b_s/b_{bB} in terms of γ (Fig.5.b) suggests *in situ* particles have refractive indices significantly lower than the Mie-theoretically estimated refractive indices for similar ranges of b_s/b_b. The use of the random-shape inversion model in our calculation of γ likely has limited the overestimation of small particles concentration, as obtained from Mie-based model (not shown here) [10].

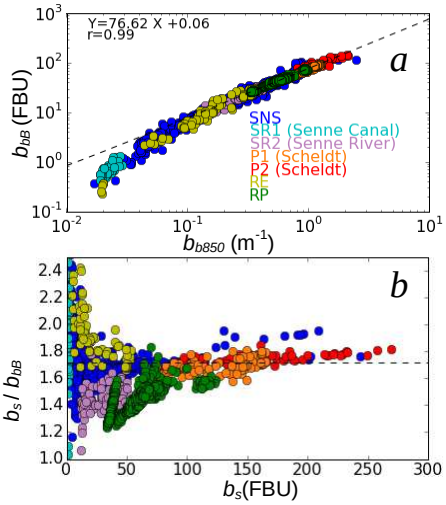

Figure 4. From OBS and HS4 (station and continuous) measurement sites: a) b_{bB} versus b_{b850}, b) the ratio b_s/b_{bB} versus b_s.

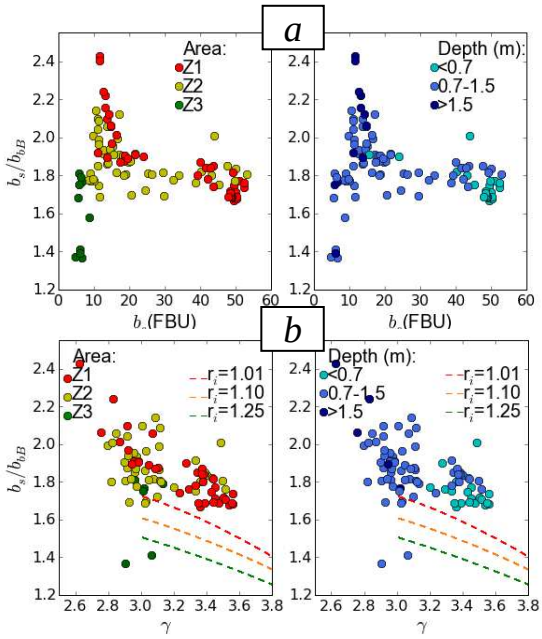

Figure 5. a) The ratio b_s/b_{bB} versus b_s from in situ *measurements at RE site, b) b_s/b_{bB} versus Junge parameter γ, estimated from* in situ *measurements at RE (coloured circles), and b_s/b_b versus γ from Fournier-Forand simulations at three refractive indices (dashed lines). The colours of the symbols relate the positions of stations as in Fig.1 (left) and to measurement depth (right).*

In the areas Z1 and Z2, sediment particles from terrigenous origin (river load) are more likely to dominate, while coarser algae-dominated particles dominate in the area Z3 (the farthest from the Rhône estuary) [11] which is corroborated by Fig.5.b: the variation of the simulated b_s/b_b in terms of refractive

indices suggests that particles in Z1-Z2 have generally higher refractive indices than the particles in Z3. The measurements in Z1 present relatively more particles with small size (γ>3.3) than in the area Z1.

Very low γ values are obtained from measurements in the three Rhône zones Z1-Z3, down to 2.6, which is lower than the values reported for the open sea, but agree with estimations reported for coastal waters [8]. Discarding out-of-range finer particles (<2.7µm) from γ calculation could have affected the accuracy of LISST derived PSD, shifting γ towards smaller ranges (larger particles concentration). On the other hand, higher values up to 3.56 were estimated mostly from measurements made just below the water surface (depth≤0.7m). Note that these high γ values may have been biased by stray light effects encountered near the sea surface [12], [13].

Fig.6 presents the ratio b_s/b_b obtained from the simulated VSF. The b_s/b_b decreases at a rate of 56% from 1.70 to 0.75 with γ increasing from 3.2 to 5, for particles with small refractive indices (<1.1). For higher refractive indices the variability of b_s/b_b value for increasing γ is slightly reduced (e.g. 48% at r_i=1.3, and 45% at r_i=1.53). For high γ>4.8, b_s/b_b values almost do not vary with increasing refractive index (only by a factor less than 5%), and that variation increases slowly with decreasing γ. In the lower range, γ<3.4, the maximum percentage variation of b_s/b_b is 20%.
While the refractive index is the main factor that impacts the backscattering ratio b_b/b, where b is the total scattering coefficient [14], [15], our simulations indicate that the particle size distribution is the main factor contributing to variations in b_s/b_b.

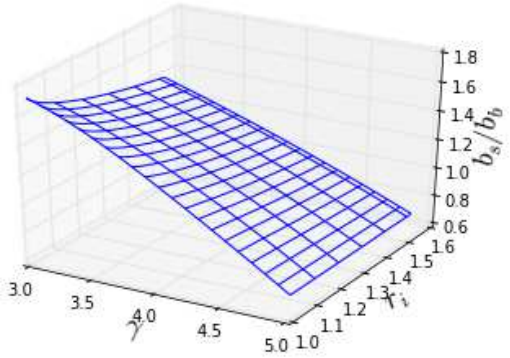

Figure 6. The ratio b_s/b_b estimated from Fournier-Forand scattering phase function, in terms of the Junge parameter and the refractive index.

4. CONCLUSION AND PERSPECTIVES

The turbidity model [1] is recalibrated and validated proving its applicability to a large range of turbidity from moderate to extremely turbid waters (10-1500 FNU). The calibration coefficients are provided for a hyperspectral sensor as well as for the Sentinel-2 MSI, Pléiades and Landsat8 OLCI sensors.

The relationship between *in situ* side- and back-scattering coefficients shows a large variability of the ratio b_s/b_b in the lower turbidity range (<20 FNU). However, this variability decreases drastically with increasing turbidity indicating the predominance of particles with less heterogeneity as regard their type/composition and size. Simultaneous OBS and LISST measurements shed light on the important part played by PSD in the variability of b_s/b_b: particles from the same areas (indicating similar origin, type and composition) exhibit a b_s/b_b ratio which decreases with increasing Junge power, i.e. with finer particles that dominate the water mass. This is corroborated by Fournier-Forand simulations, which further indicate that for a given particle size, b_s/b_b decreases with increasing refractive index.

For *in situ* measurements, accurate retrieval of PSD and refractive indices can be performed by means of improved models for inversion of the volume scattering function, with a better representation of various shapes of particles e.g. [16].

From a remote-sensing perspective, the retrieval of the side-scattering coefficient (using a turbidity model) and backscattering coefficient (by inversion of the reflectance model, e.g. QAA model) from marine reflectance can help providing information on particles refractive index, by inspecting the variability of the side- to back-scattering ratio with particle size.

5. ACKNOWLEGDMENTS

This work was carried out in the frame of the European Space Agency (ESA) FP7/2007-2013, under grant agreement n° 606797 (HIGHROC project), with the support from LOV-CNRS under contract ANR-MATUGLI for the Rhône River plume campaign, and with the participation of the Belgian Science Policy Office (BELSPO) for funding of the TURBINET project PIP-2012/350 and PICT-2014/0455, which supported the in-water continuous OBS measurements in Argentina and Belgium. Special thanks are directed to the RV Belgica captains and crews (2007-2015) who hosted the majority of the SNS campaigns; to the Fishermen's pier crew for support and access to the pier in Río de la Plata site in Argentina; to the Waterwegen en Zeekanaal NV (especially Sven Deckers) for help with administrative and logistical aspects, that made possible the measurements at the Kallebeek, Antwerp and Machelen sites in Belgium; to Anouck Ody for her help with measurements in the Rhône River plume, and to Sabine Marty for the pre-processing of the LISST measurements in the Rhône River plume site.

6. REFERENCES

[1] B. Nechad, K.G. Ruddick, G. Neukermans, "Calibration and validation of a generic multisensor algorithm for mapping of turbidity in coastal waters," *SPIE Eur. Int. Symp. Remote Sens. Berl.*, 2009.

[2] E. Boss, L. Taylor, S. Gilbert, K. Gundersen, N. Hawley, C. Janzen, T. Johengen, H. Purcell, C. Robertson, D. W. H. Schar, G. J. Smith, and M. N. Tamburri, "Comparison of inherent optical properties as a surrogate for particulate matter concentration in coastal waters: Optical properties as proxies of particulate matter," *Limnol. Oceanogr. Methods*, vol. 7, no. 11, pp. 803–810, Nov. 2009.

[3] A. I. Dogliotti, K. G. Ruddick, B. Nechad, D. Doxaran, and E. Knaeps, "A single algorithm to retrieve turbidity from remotely-sensed data in all coastal and estuarine waters," *Remote Sens. Environ.*, vol. 156, pp. 157–168, Jan. 2015.

[4] C. D. Mobley, "Estimation of the remote-sensing reflectance from above-surface measurements," *Appl. Opt.*, vol. 38, no. 36, p. 7442, Dec. 1999.

[5] K. G. Ruddick, V. De Cauwer, Y.-J. Park, and G. Moore, "Seaborne measurements of near infrared water-leaving reflectance: The similarity spectrum for turbid waters," *Limnol. Oceanogr.*, vol. 51, no. 2, pp. 1167–1179, Mar. 2006.

[6] G. Neukermans, H. Loisel, X. Mériaux, R. Astoreca, and D. McKee, "In situ variability of mass-specific beam attenuation and backscattering of marine particles with respect to particle size, density, and composition," *Limnol. Oceanogr.*, vol. 57, no. 1, pp. 124–144, 2012.

[7] D. Doxaran, E. Leymarie, B. Nechad, A. Dogliotti, K. Ruddick, P. Gernez, and E. Knaeps, "Improved correction methods for field measurements of particulate light backscattering in turbid waters," *Opt. Express*, vol. 24, no. 4, p. 3615, Feb. 2016.

[8] A. Jouon, S. Ouillon, P. Douillet, J. P. Lefebvre, J. M. Fernandez, X. Mari, and J.-M. Froidefond, "Spatio-temporal variability in suspended particulate matter concentration and the role of aggregation on size distribution in a coral reef lagoon," *Mar. Geol.*, vol. 256, no. 1–4, pp. 36–48, Dec. 2008.

[9] M. Babin, A. Morel, V. Fournier-Sicre, F. Fell, and D. Stramski, "Light scattering properties of marine particles in coastal and open ocean waters as related to the particle mass concentration," *Limnol. Oceanogr.*, vol. 48, no. 2, pp. 843–859, Mar. 2003.

[10] Y. C. Agrawal, A. Whitmire, O. A. Mikkelsen, and H. C. Pottsmith, "Light scattering by random shaped particles and consequences on measuring suspended sediments by laser diffraction," *J. Geophys. Res.*, vol. 113, no. C4, Apr. 2008.

[11] T. Lorthiois, D. Doxaran, and M. Chami, "Daily and seasonal dynamics of suspended particles in the Rhône River plume based on remote sensing and field optical measurements," *Geo-Mar. Lett.*, vol. 32, no. 2, pp. 89–101, Apr. 2012.

[12] R. A. Reynolds, D. Stramski, V. M. Wright, and S. B. Woźniak, "Measurements and characterization of particle size distributions in coastal waters," *J. Geophys. Res.*, vol. 115, no. C8, Aug. 2010.

[13] S. Andrews, D. Nover, and S. G. Schladow, "Using laser diffraction data to obtain accurate particle size distributions: the role of particle composition: Laser diffraction data processing," *Limnol. Oceanogr. Methods*, vol. 8, no. 10, pp. 507–526, Oct. 2010.

[14] E. Boss, "Particulate backscattering ratio at LEO 15 and its use to study particle composition and distribution," *J. Geophys. Res.*, vol. 109, no. C1, 2004.

[15] M. S. Twardowski, E. Boss, J. B. Macdonald, W. S. Pegau, A. H. Barnard, and J. R. V. Zaneveld, "A model for estimating bulk refractive index from the optical backscattering ratio and the implications for understanding particle composition in case I and case II waters," *J. Geophys. Res. Oceans*, vol. 106, no. C7, pp. 14129–14142, Jul. 2001.

[16] X. Zhang, M. Twardowski, and M. Lewis, "Retrieving composition and sizes of oceanic particle subpopulations from the volume scattering function," *Appl. Opt.*, vol. 50, no. 9, p. 1240, Mar. 2011.